Two-Dimensional Penning Ionization Electron Spectroscopy of Monohalogenobenzenes by He*(2^3S): C_6H_5X (X = F, Cl, Br, I)

Kohei Imura, Naoki Kishimoto, and Koichi Ohno*

Department of Chemistry, Graduate School of Science, Tohoku University, Aramaki, Aoba-ku, Sendai 980-8578, Japan

Received: December 7, 2000; In Final Form: February 6, 2001

Penning ionization of C_6H_5X (X = F, Cl, Br, I) upon collision with metastable He*(2^3S) atoms was studied by two-dimensional (collision-energy/electron-energy-resolved) Penning ionization electron spectroscopy. Partial ionization cross sections are found to be larger for ionization from orbitals having n and π characters. Interaction potentials between the target molecule and the He* atom were found to be highly anisotropic. Attractive interaction was dominated around the collinear access of He*(2^3S) to C−F axis in C_6H_5F. On the other hand, attractive interaction was localized around the out-of-plane perpendicular approach of He* atom to C−X bond (X = Cl, Br, I). Attractive interaction for these compounds increases on going from C_6H_5Cl to C_6H_5I. Furthermore, the electronic factor due to the size of the halogen p orbitals and the conjugation between the benzene ring and the halogen atoms and also the steric factor due to the shielding effect were found to be important.

I. Introduction

It is well-known that shape and spread of molecular orbitals play the central role in the chemical reaction. Penning ionization electron spectroscopy is one of the most suitable methods for probing electron distributions of molecular orbitals (MOs). Penning ionization[1] can occur when a molecule M collides with a metastable atom A* ($A^* + M \rightarrow A + M^+ + e^-$).

The Penning ionization process can be explained by the electron exchange model, in which overlap of orbitals related to the electron exchange is required.[2] Ohno et al.[3,4] successfully applied the exterior electron density (EED) model to this process in order to account for experimental branching ratios of Penning ionization. Based on this model, Penning ionization partial cross sections can be roughly simulated by the EED, electron distribution of target MOs exposed outside the molecular surface, which is approximated by the van der Waals radii. Then, larger electron distribution outside the molecular surface brings larger overlap of mutual orbitals involving electron exchange with resultant large ionization probability. Therefore the reaction probability depends on both the electron distribution of the target MO and the interaction potentials, since the electron distributions of the target MOs have anisotropic distributions. The kinetic energy of the ejected electron depends on the energy difference between the entrance potential energy surface of $A^* + M$ and the exit potential energy surface of $A + M^+$ at the ionization point.[5] Thus Penning ionization electron spectroscopy does not give the ionization potential (IP) of the isolated molecule, which can be determined by He I ultraviolet photoelectron spectroscopy. Then there are small kinetic energy shifts compared with Penning ionization electron spectrum (PIES) and He I ultraviolet photoelectron spectrum (UPS), depending on the energy difference between the metastable atom and the photon energy. The information on the interaction potential of the entrance channel can be obtained from the peak energy shift if the exit potential can be assumed as flat in the ionization region. A positive peak energy shift implies that the interaction is repulsive. Contrary, a negative shift can be ascribed to the attractive interaction.

Branching ratio of PIES is determined by the partial ionization cross sections. In many cases, attractive interactions enhance the ionization cross section, while there are some exceptions such as n_O orbital in the carbonyl group.[6] On the contrary, repulsive interactions decrease the ionization cross section. It is obvious that the ionization cross section depends not only on the characteristic of the interaction but also on collision energy of the metastable atom. Two-dimensional (2D) PIES has been recently developed in our laboratory,[7] in which ionization cross sections are determined as functions of both electron kinetic energy (E_e) and metastable atom collision energy (E_c). This technique makes it possible to study the collision energy dependence of the partial ionization cross sections (CEDPICS) and collision-energy-resolved PIES (CERPIES), and thus the state-resolved measurement of partial cross sections for the *i*th ionic state enables us to investigate anisotropy potential surface around the target molecule. 2D-PIES studies of several aromatic compounds (such as benzene,[8] polycyclic aromatic hydrocarbons,[9] heterocyclic compounds,[10] [2,2]-paracyclophane,[11] azines,[12] and substituted benzenes[13] (aniline, phenol, thiophenol) with He(2^3S) atoms have been reported so far.

Anisotropic interaction around Cl atoms in several molecules[14−19] with metastable atoms has been discussed. Very recently, Imura et al.[20] have studied the anisotropic interaction of halogen atoms in C_2H_5X (X = Cl, F) with He*(2^3S). We found a very different trend in the interaction around C−X (X = Cl, F); attractive interaction was dominated around the perpendicular directions to the C−Cl bond axis, while for the C−F bond attractive interaction was localized around the collinear axis.

From a chemical point of view, it is very interesting and important to reveal the interaction feature of atoms, which have same number of valence electrons. Because it is well-known that atoms having the same number of valence electrons such as halogen atoms show similar and systematic chemical

10.1021/jp004430n CCC: $20.00
Published on Web 04/07/2001

characteristics in many reaction systems from a macroscopic point of view. One question can be raised from a microscopic point of view whether the reaction dynamics of these species are similar or not. Furthermore, the Penning ionization process is regarded as an electrophilic reaction of an excited atom A* with a molecule M; the reagent A* attacks an orbital of M and extracts an electron into the vacant orbital of A* yielding an ionic state of M^+. In this respect, 2D-PIES of the target molecules with the metastable atoms enable us to investigate the reactivity and anisotropic interaction of the target MO in the electrophilic reactions.

In this paper, we have measured 2D-PIES of C_6H_5X (X = F, Cl, Br, I) in order to get insight about the anisotropic interaction around these halogen atoms and to obtain systematic understanding for reactivity and anisotropic interaction of the n and π orbitals of monohalogenobenzenes. Such a study is of a considerable chemical significance because it provides insight into the role of the n and π orbitals in electrophilic reactions of the compounds.

II. Experimental Section

High purity samples C_6H_5X (X = F, Cl, Br, I) (F, Cl, Br > 99.5% and I > 98%) were commercially purchased and used after several freeze−pump−thawed cycles. The experimental apparatus for He*(2^3S) Penning ionization electron spectroscopy has been reported previously.[8,17,21,22] The metastable He* beam was generated by a discharge nozzle source with a tantalum hollow cathode. The metastable He* atoms in the 2^1S state are optically removed by the helium discharge (quench) lamp after passing through the skimmer. Ionic and Rydberg species produced by the discharge were removed by the electric deflector. The He*(2^3S) metastable beam enters into the collision cell where sample gas was introduced. Produced electrons by the Penning ionization were measured by a hemispherical electrostatic deflection type analyzer using an electron collection angle 90° to the incident He* beam. He I UPS were measured by using the He I resonance photons (584 nm, 21.22 eV) produced by dc-discharge in pure helium gas. The kinetic energy of ejected electrons was measured by the analyzer using an electron collection angle 90° to the incident photon beam. The energy resolution of the electron energy analyzer was estimated to be 70 meV from the full width at the half-maximum (fwhm) of the $Ar^+(^2P_{3/2})$ peak in the He I UPS. The transmission efficiency curve of the electron analyzer was determined by comparing our UPS data of several molecules with those by Gardner and Samson[23] and Kimura et al.[24] Calibration of the electron energy scale was made by reference to the lowest ionic state of N_2 mixed with the sample molecule in He I UPS (E_e = 5.639 eV)[25] and He* (2^3S) PIES (E_e = 4.292 eV).[26,27]

In the collision-energy-resolved experiments, 2D-PIES, the metastable atom beam was modulated by a pseudorandom chopper[28] rotating about 400 Hz and introduced into the reaction cell located at 504 mm downstream from the chopper disk with keeping constant sample pressure. The resolution of the electron analyzer was lowered to 250 meV in order to gain higher electron counting rates. Time-dependent electron signals for each kinetic electron energy (E_e) were recorded with scanning electron energy of a 35 meV step. The 2D Penning ionization data as functions of both E_e and t were stored in a memory of a computer. The velocity dependence of the electron signals was obtained from the time-dependent signals by Hadamard transformation in which time-dependent signals were cross-correlated with the complementary slit sequence of the pseudorandom chopper. Similarly, velocity distribution of metastable He* beam was determined by measuring the intensity of secondary emitted electrons from the inserted stainless steel plate. The 2D Penning ionization cross section $\sigma(E_e, v_r)$ was obtained with normalization by the velocity distribution of He* $I_{He^*}(v_{He^*})$.

$$\sigma(E_e, v_r) = A[I_e(E_e, v_{He^*})/I_{He^*}(v_{He^*})](v_{He^*}/v_r)$$

$$v_r = [v_{He^*}^2 + 3kT/M]^{1/2}$$

where A, v_r, k, T, and M are proportionality constants, the relative velocity of metastable atoms averaged over the velocity of the sample molecule, the Boltzmann constants, the gas temperature (300 K), and the mass of the sample molecule, respectively. Finally, $\sigma(E_e, v_r)$ is converted to $\sigma(E_e, E_c)$ as functions of E_e and E_c by the following relation:

$$E_c = \mu v_r^2/2$$

where μ is the reduced mass of the reaction system.

III. Calculations

We performed ab initio self-consistent field (SCF) calculations with either 4-31G basis functions for C_6H_5F and C_6H_5Cl or 6-311G for C_6H_5Br and C_6H_5I in order to obtain electron density contour maps of MOs. The geometries of the molecules were used from microwave spectroscopic studies.[29−32] In electron density maps, thick solid curves indicate the repulsive molecular surface approximated by van der Waals radii[33] (r_C = 1.7 Å, r_H = 1.2 Å, r_F = 1.35 Å, r_{Cl} = 1.8 Å, r_{Br} = 1.95 Å, r_I = 2.15 Å).

Interaction potential energies between He*(2^3S) and M in various directions and angles were also calculated on the basis of the well-known resemblance between He*(2^3S) and Li(2^2S);[34] the shape of the velocity dependence of the total scattering cross section of He*(2^3S) by He, Ar, and Kr is very similar to that of Li, and the location of the interaction potential well and its depth are similar for He*(2^3S) and Li with various targets.[35−38] Because of these findings and the difficulties associated with calculation for excited states, Li was used in this study in place of He*(2^3S). Thus the interaction potential M−Li(2^2S), $V^*(R,\theta)$ (where R is either Li−X distance or the distance from the center of the benzene ring and θ is in-plane angle of ∠Li−X−C), was calculated by moving the Li atom toward the halogen atom and keeping the molecular geometries fixed at the experimental values; this assumption meant that the geometry change by the approach of a metastable atom was negligible in the collisional ionization process. For calculating the interaction potential, standard 6-31+G* basis set was used, and the correlation energy correction was partially taken into account by using second-order Møller−Plesset perturbation theory (MP2). All calculations in this study were performed with the GAUSSIAN 98 quantum chemistry program.[39] The ionization potentials were calculated at the experimentally determined geometries using the outer valence Green's function (OVGF) method[40,41] for C_6H_5X (X = F, Cl, Br) with 6-31+G* basis sets and for C_6H_5I with CEP-4-31G as incorporated in GAUSSIAN 98.

IV. Results

Figures 1−4 show the He I UPS and He*(2^3S) PIES of C_6H_5F, C_6H_5Cl, C_6H_5Br, and C_6H_5I, respectively. The electron energy scale for PIES are shifted relative to those of UPS by the excitation energy difference between He I photons (21.22 eV) and He*(2^3S) (19.82 eV), namely, 1.40 eV. The present He I UPS and He*(2^3S) PIES are consistent with the earlier

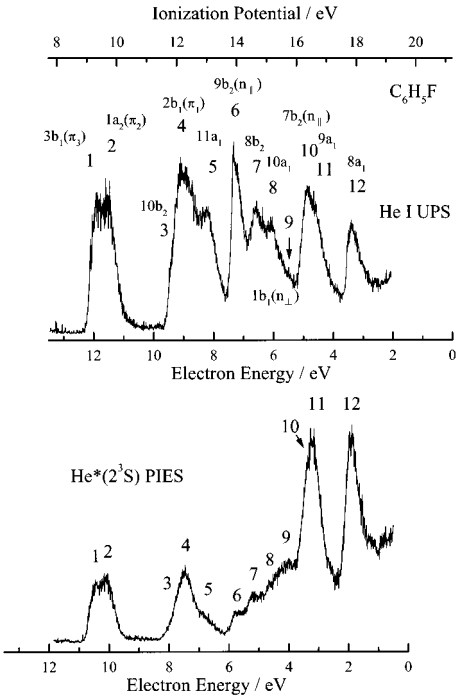

Figure 1. He I UPS and He(2^3S) PIES of C_6H_5F. Average collision energy (60−400 meV) of PIES was $E_c \sim 160$ meV.

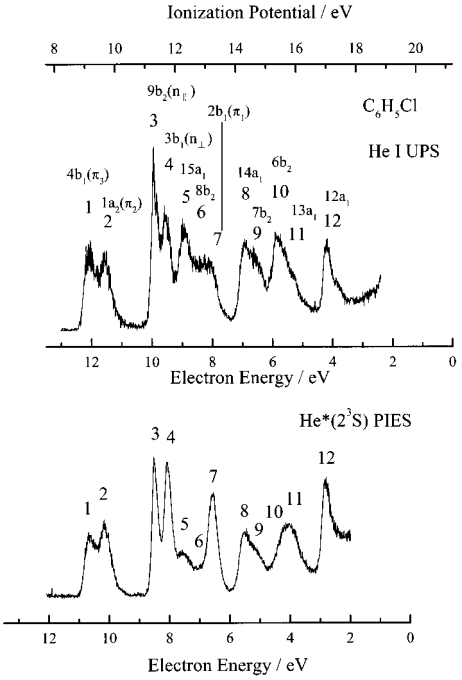

Figure 2. He I UPS and He(2^3S) PIES of C_6H_5Cl. Average collision energy (60−400 meV) of PIES was $E_c \sim 160$ meV.

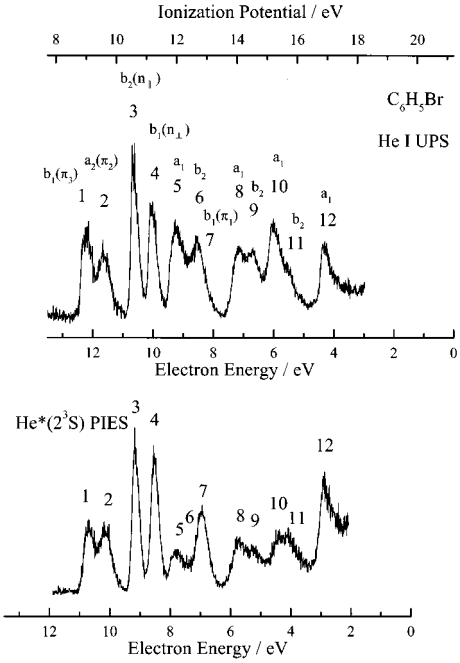

Figure 3. He I UPS and He(2^3S) PIES of C_6H_5Br. Average collision energy (60−400 meV) of PIES was $E_c \sim 160$ meV.

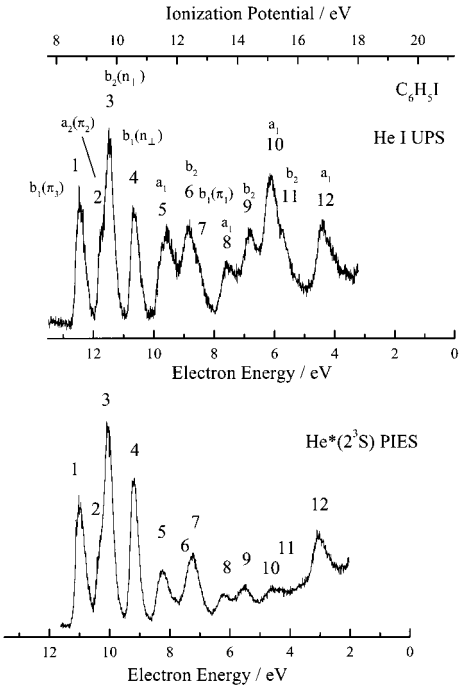

Figure 4. He I UPS and He(2^3S) PIES of C_6H_5I. Average collision energy (60−400 meV) of PIES was $E_c \sim 160$ meV.

data while there are some contradictions with the band assignments.[24,42−45] Band labels in UPS show orbital characters based on their symmetries. π_3 and π_1 orbitals are derived from the splitting of the $1e_{1g}$ orbital of benzene, while the π_1 orbital is related to the benzene $1a_{2u}$ orbital. $n_{||}$ and $n_\perp$ orbitals denote nonbonding characters due to the halogen p orbital distributed parallel and perpendicular to the benzene ring, respectively.

Figures 5−8 show the collision-energy-resolved PIES (CER-PIES) obtained from the 2D spectra of C_6H_5F, C_6H_5Cl, C_6H_5Br, and C_6H_5I, respectively. Hot spectra at the higher collision energy (ca. 250 meV) are shown by dashed curves, and the cold ones at the lower collision energy (ca. 90 meV) are shown by solid curves. Relative intensities of the two spectra are normalized in the figures using the data of the log σ vs log E_c plots.

Figures 9−12 show the log σ versus log E_c plots of CEDPICS in a collision energy range of 90−300 meV for C_6H_5F, C_6H_5Cl, C_6H_5Br, and C_6H_5I, respectively. The CEDPICS was obtained from the 2D-PIES $\sigma(E_e,E_c)$ within an appropriate range of E_e(typically electron energy resolution of analyzer, 250 meV) to avoid the contribution from neighbor bands. Electron density maps are also shown in the figures in order to grasp effective access direction of He*. The calculated electron density maps for s orbitals are shown on the molecular plane, and those for p orbitals are shown on a plane at a height of 1.7 Å (van der

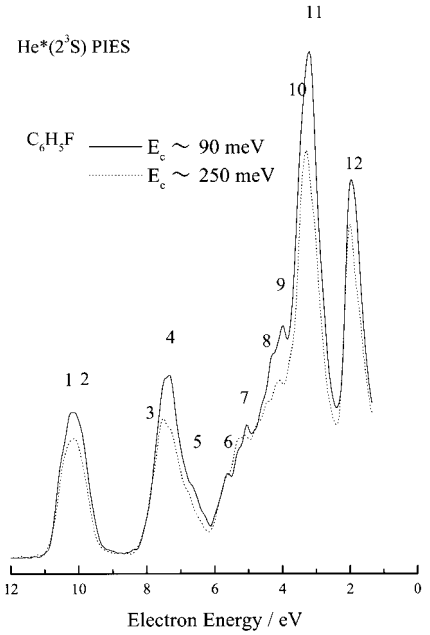

Figure 5. Collision-energy-resolved He(2^3S) PIES of C_6H_5F. E_c denotes collision energy.

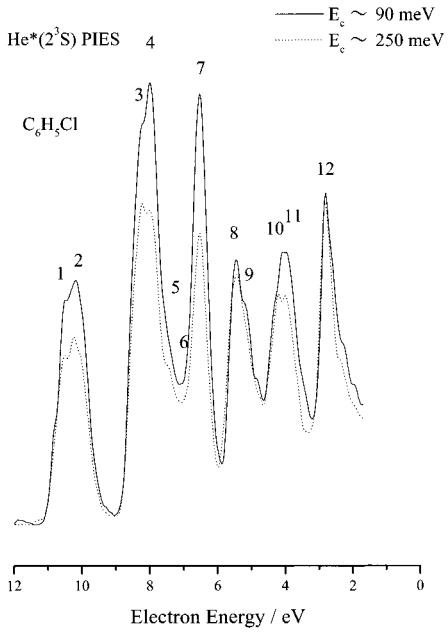

Figure 6. Collision-energy-resolved He(2^3S) PIES of C_6H_5Cl. E_c denotes collision energy.

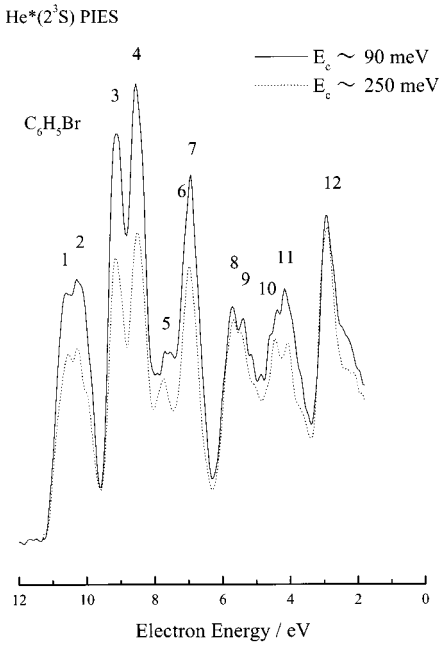

Figure 7. Collision-energy-resolved He(2^3S) PIES of C_6H_5Br. E_c denotes collision energy.

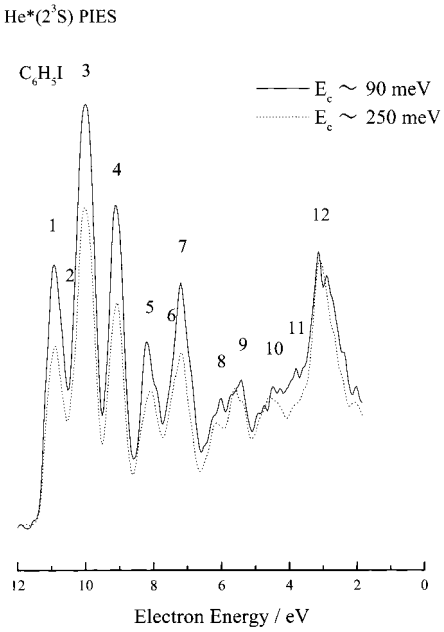

Figure 8. Collision-energy-resolved He(2^3S) PIES of C_6H_5I. E_c denotes collision energy.

Waals radii of C atom) from the molecular plane. At the right side of the figures, electron density maps for π_1, π_3, and $n_\perp$ orbitals were drawn on the symmetry plane perpendicular to the molecular plane, while electron density maps for π_2 orbitals were drawn on a plane including the center of the benzene ring and being perpendicular to both the symmetry plane and the molecular plane.

Figures 13−15 show calculated interaction potential energy curves between a ground-state Li atom and C_6H_5F, C_6H_5Cl, and C_6H_5Br, respectively. The potential curves are shown as a function of (a) the distance R between Li and either the halogen atom or the center of the benzene ring, and (b) the ∠Li−X−C angle. Calculations were performed at the MP2/6-31+G* level of theory. Interaction potential energy curves between a Li atom and C_6H_5I could not be calculated, since the proper basis set was not available to investigate the systematic and qualitative understanding of interaction potential between a Li atom and the investigated molecules. In the present study, although absolute value of potential energy might be different from the real one within several hundreds meV, systematic and qualitative understanding can be obtained from the calculated interaction potentials.

Tables 1−4 summarize experimentally observed and calculated ionization potentials (IPs), experimental peak energy shift (ΔE), slope parameters of CEDPICS (m), and the assignment of the bands. Slope parameters are obtained from the log σ vs log E_c plots in a collision energy range for 90−300 meV by a least-squares method. Vertical IPs are determined from He I UPS. The peak energy shifts are obtained as the difference between the peak position (E_{PIES}; electron energy scale) and the "nominal" value (E_0 = difference between metastable excitation energy and sample IP): $\Delta E = E_{PIES} - E_0$.

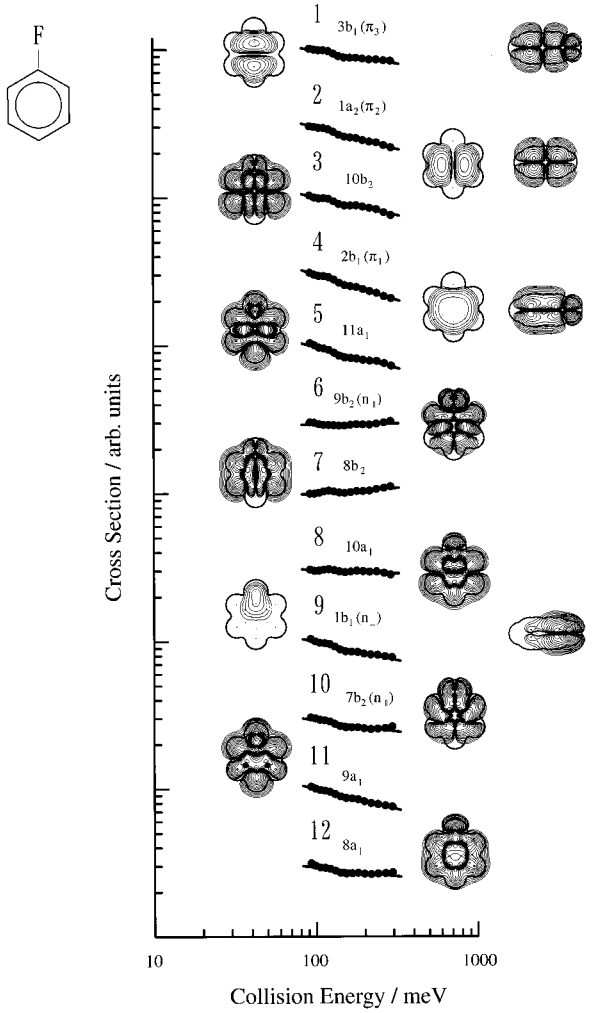

Figure 9. Collision energy dependence of partial ionization cross sections for C_6H_5F with He(2^3S) atom. The contour plots show electron density maps for respective MOs.

TABLE 1: Band Assignment, Ionization Potentials (IP/eV), Peak Energy Shifts (Δ*E*/meV), and Slope Parameters (*m*) C_6H_5F

molecule	band	IP_{obsd}/eV	IP_{OVGF}/eV (pole strength)	orbital character	Δ*E*/meV	*m*
C_6H_5F	1	9.29	9.02(0.90)	$3b_1(\pi_3)$	-90 ± 70	−0.18
	2	9.74	9.35(0.90)	$1a_2(\pi_2)$	0.0 ± 70	−0.22
	3	11.85	12.30(0.84)	$10b_2$	-180 ± 120	−0.24
	4	12.13	12.26(0.91)	$2b_1(\pi_1)$	-230 ± 80	−0.34
	5	12.98	12.88(0.90)	$11a_1$	$(+50 \pm 120)$	−0.28
	6	13.90	14.22(0.89)	$9b_2(n_{\|\|})$	-70 ± 90	+0.01
	7	14.64	14.69(0.89)	$8b_2$	$+40 \pm 90$	+0.07
	8	15.18	15.21(0.88)	$10a_1$	-10 ± 80	−0.05
	9	15.8	16.49(0.87)	$1b_1(n_\perp)$	(-100 ± 150)	−0.24
	10	16.35	16.82(0.87)	$7b_2$	-50 ± 100	−0.15
	11	16.64	16.64(0.87)	$9a_1$	-40 ± 80	−0.24
	12	17.84	18.23(0.86)	$8a_1(\sigma_{CF})$	-30 ± 70	−0.12

V. Discussion

UPS and PIES of C_6H_5X (X = F, Cl, Br, I) have been reported. Band assignments in UPS have been reported on the basis of the relative intensity of the corresponding bands in PIES.[45] In the present study, we obtained consistent results with them from experiment and theoretical calculations except for C_6H_5F, in which assignments of band 9 and 11 have slightly modified from the previous study[45] based on the latter discussions and also on the results of OVGF calculation. In addition,

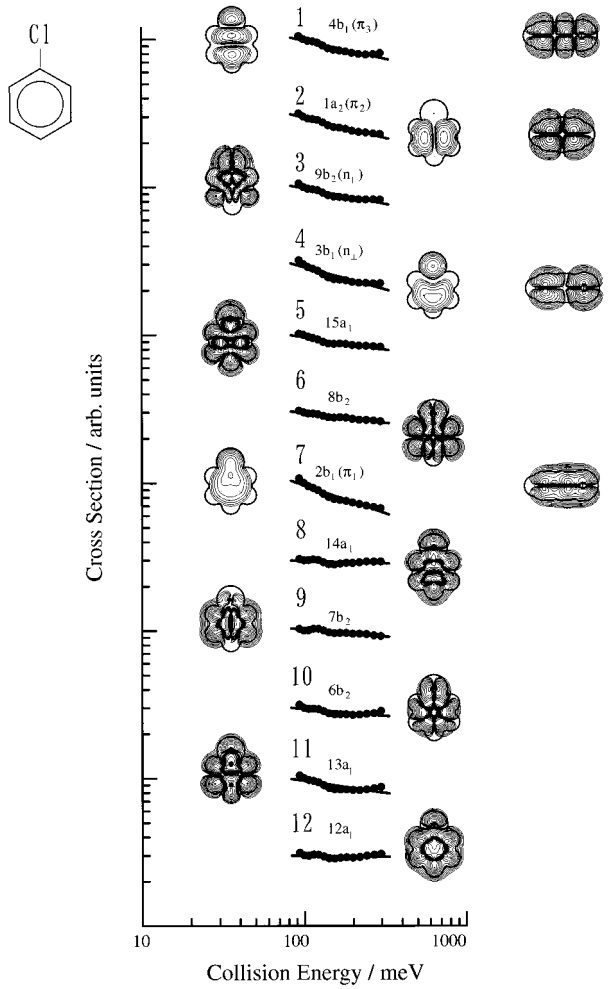

Figure 10. Collision energy dependence of partial ionization cross sections for C_6H_5Cl with He(2^3S) atom. The contour plots show electron density maps for respective MOs.

TABLE 2: Band Assignment, Ionization Potentials (IP/eV), Peak Energy Shifts (Δ*E*/meV), and Slope Parameters (*m*) C_6H_5Cl

molecule	band	IP_{obsd}/eV	IP_{OVGF}/eV (pole strength)	orbital character	Δ*E*/meV	*m*
C_6H_5Cl	1	9.05	8.82(0.90)	$4b_1(\pi_3)$	-90 ± 80	−0.24
	2	9.65	9.32(0.90)	$1a_2(\pi_2)$	-30 ± 80	−0.27
	3	11.28	11.23(0.91)	$9b_2(n_{\|\|})$	(-40 ± 50)	−0.21
	4	11.65	11.63(0.88)	$3b_1(n_\perp)$	-100 ± 50	−0.30
	5	12.30	12.44(0.90)	$15a_1$	$(+40 \pm 60)$	−0.17
	6	12.95	12.49(0.90)	$8b_2$	(-50 ± 100)	(−0.13)
	7	13.11	13.22(0.84)	$2b_1(\pi_1)$	-150 ± 60	−0.37
	8	14.30	14.51(0.89)	$14a_1$	$+10 \pm 70$	−0.03
	9	14.63	14.63(0.89)	$7b_2$	(-70 ± 100)	−0.09
	10	15.35	15.39(0.87)	$6b_2$	(-200 ± 100)	−0.09
	11	15.64	15.90(0.88)	$13a_1$	(-160 ± 120)	−0.16
	12	17.02	17.37(0.86)	$12a_1$	$+20 \pm 50$	−0.01

we obtained the almost coincident results of the relative intensities of the π and n orbitals for these compounds. Slight discrepancy between the present study and the previous work[45] can be ascribed to the difference of collision energy. This finding suggests that the CEDPICS for these bands should be similar each other. Observed features of PIES for these compounds are summarized as follows.

The enhancement of π bands in PIES was observed in accord with the other conjugated molecules.[3,4] As can be seen from Figures 13−15, attractive interactions were found for the perpendicular directions to the center of the benzene ring (●).

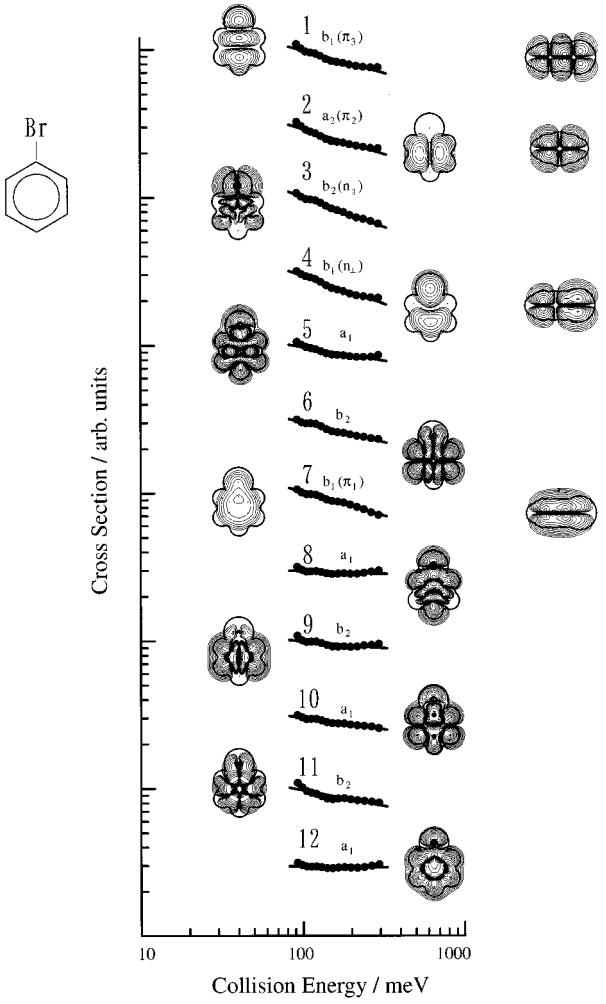

Figure 11. Collision energy dependence of partial ionization cross sections for C_6H_5Br with He(2^3S) atom. The contour plots show electron density maps for respective MOs.

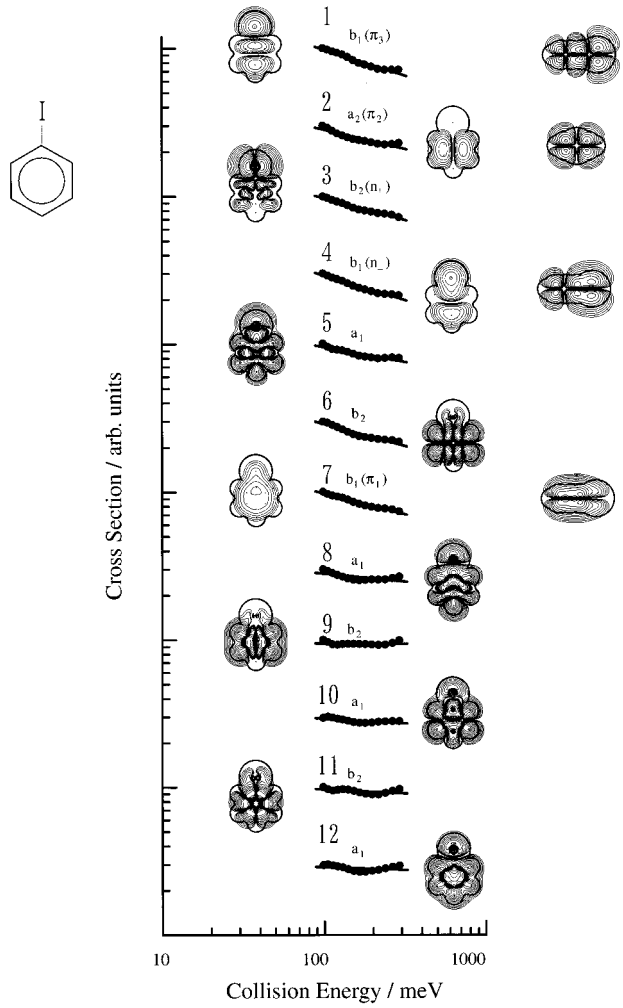

Figure 12. Collision energy dependence of partial ionization cross sections for C_6H_5I with He(2^3S) atom. The contour plots show electron density maps for respective MOs.

TABLE 3: Band Assignment, Ionization Potentials (IP/eV), Peak Energy Shifts (Δ*E*/meV), and Slope Parameters (*m*) C_6H_5Br

molecule	band	IP_{obsd}/eV	IP_{OVGF}/eV (pole strength)	orbital character	Δ*E*/meV	*m*
C_6H_5Br	1	9.00	8.66(0.90)	$b_1(\pi_3)$	-120 ± 100	-0.30
	2	9.63	9.30(0.90)	$a_2(\pi_2)$	-140 ± 100	-0.34
	3	10.53	10.61(0.91)	$b_2(n_{\|\|})$	-180 ± 60	-0.41
	4	11.19	11.12(0.89)	$b_1(n_\perp)$	-150 ± 60	-0.38
	5	11.95	12.18(0.90)	a_1	-50 ± 80	-0.18
	6	12.68	12.32(0.90)	b_2	-60 ± 100	(-0.27)
	7	12.96	12.84(0.83)	$b_1(\pi_1)$	(-50 ± 140)	-0.32
	8	14.06	14.09(0.89)	a_1	-30 ± 90	-0.03
	9	14.52	14.56(0.89)	b_2	-60 ± 100	-0.09
	10	15.20	15.25(0.86)	a_1	-230 ± 100	-0.15
	11	15.66	15.67(0.87)	b_2	-70 ± 120	-0.21
	12	16.85	17.23(0.86)	a_1	-50 ± 120	-0.01

TABLE 4: Band Assignment, Ionization Potentials (IP/eV), Peak Energy Shifts (Δ*E*/meV), and Slope Parameters (*m*) C_6H_5I

molecule	band	IP_{obsd}/eV	IP_{OVGF}/eV (pole strength)	orbital character	Δ*E*/meV	*m*
C_6H_5I	1	8.75	8.30(0.92)	$b_1(\pi_3)$	-80 ± 60	-0.35
	2	9.49	9.05(0.90)	$a_2(\pi_2)$	-50 ± 80	-0.26
	3	9.74	9.37(0.94)	$b_2(n_{\|\|})$	-50 ± 50	-0.29
	4	10.54	10.17(0.91)	$b_1(n_\perp)$	-80 ± 50	-0.33
	5	11.64	11.37(0.92)	a_1	$+60 \pm 100$	-0.20
	6	12.29	12.04(0.90)	b_2	(-100 ± 120)	(-0.30)
	7	12.6	12.62(0.83)	$b_1(\pi_1)$	(-30 ± 100)	-0.28
	8	13.63	13.63(0.89)	a_1	-20 ± 90	-0.11
	9	14.42	14.47(0.89)	b_2	$+60 \pm 80$	-0.01
	10	15.12	15.07(0.87)	a_1	-130 ± 70	-0.06
	11	15.48	15.34(0.88)	b_2	-30 ± 120	-0.05
	12	16.83	17.07(0.86)	a_1	$+30 \pm 100$	-0.04

These attractive interactions are responsible for the enhancement of π bands in PIES. It is noted that the depth of the potential well for this direction increases on going from C_6H_5F to C_6H_5-Br.

The n bands also show relatively large enhancement of the intensity, while it depends on the constituent halogen atoms. The change in the degrees of the enhancement on going from C_6H_5F to C_6H_5I was obtained. This is explained by a steric shielding effect of the benzene ring. It is known that such a shielding effect of bulky groups has been found in various compounds.[46−48] The strong intensities for these orbitals can be explained by the large exterior electron distribution outside the repulsive surface. The ab initio MO calculation for the out-of-plane perpendicular direction to C−X (X = Cl, Br) axis(◆) indicated that attractive interaction was dominant. As can be seen in Figure 15, larger attractive interaction was found for C_6H_5Br (−165 meV) than that for C_6H_5Cl (−54 meV).

We will further discuss the reactivity and anisotropic interaction of these compounds with He*(2^3S) on the basis of the CEDPICS for each band.

A. Fluorobenzene. Both *m* and Δ*E* for $2b_1(\pi_1)$ band are negative, and their absolute values are the largest. When a slower

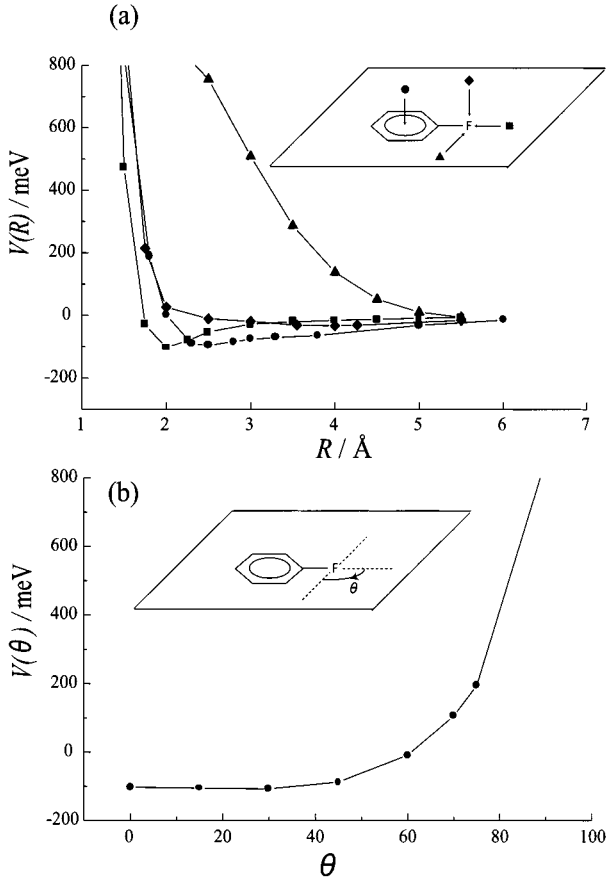

Figure 13. (a) Interaction potential curves V(R) obtained by MP2 calculations for C_6H_5F and Li as a function of distance R; out-of-plane access to the center of the benzene ring (●); in-plane collinear access to the C−F bond (■); in-plane perpendicular access to the C−F bond (▲); out-of-plane perpendicular access to the C−F bond(◆). Note that R is defined from the center of the benzene ring for (●) direction, while for the others (■), (▲), (◆) R is defined from the F atom. (b) Interaction potential curve $V(\theta)$ as a function of the in-plane angle θ of ∠Li−F−C. Distance between Li and F atoms is fixed at 2.0 Å.

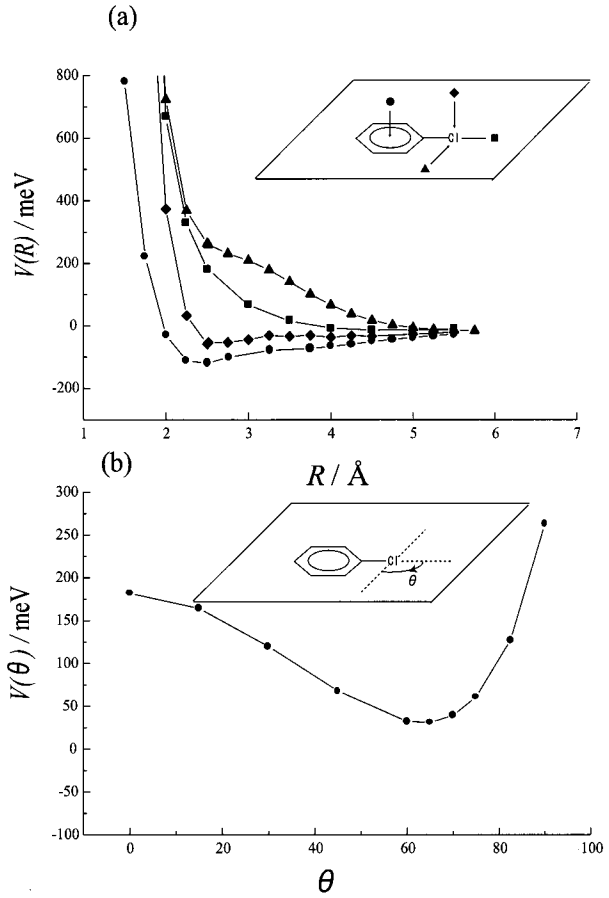

Figure 14. (a) Interaction potential curves V(R) obtained by MP2 calculations for C_6H_5Cl and Li as a function of distance R; out-of-plane access to the center of the benzene ring (●); in-plane collinear access to the C−Cl bond (■); in-plane perpendicular access to the C−Cl axis (▲); out-of-plane perpendicular access to the C−Cl axis (◆). Note that R is defined from the center of the benzene ring for (●) direction, while for the others (■), (▲), (◆) R is defined from the Cl atom. (b) Interaction potential curve $V(\theta)$ as a function of the in-plane angle θ of ∠Li−Cl−C. Distance between Li and Cl atoms is fixed at 2.5 Å.

He* metastable atom can approach the reactive region effectively by attractive force, ionization cross section is enhanced for lower collision energies. Negative slope parameter, which indicates a decrease of ionization reactivity with increase of collision energy, is consistent with the negative peak energy shift. It indicates that π_1 orbital shows the largest attractive interaction with He*(2^3S) owing to the character of the π orbital widely distributed outside the molecular surface. The electron density map shown in the right side of Figure 9 indicates that the π orbitals are exposed to the outside beyond the van der Waals radii illustrated by solid curves. Then relatively large absolute values of the m and ΔE for $1a_2(\pi_2)$ and $3b_1(\pi_3)$ bands can also be explained by the same argument. However, those values are slightly smaller than that of the π_1 orbital. It can be explained as follows. The strongest attractive interaction localized more or less around the center of the benzene ring, while these orbitals have less electron distribution owing to the nodal plane around the center of the ring. Bands of $11a_1$, $10a_1$, $9a_1$, and $8a_1$ show negative slope parameters. Change in the degrees of the slope parameters among these bands depends on the contribution of attractive interaction around the F atom and repulsive interaction around C−H bonds. As can be seen in Figure 9, $11a_1$ and $9a_1$ orbitals have larger electron distribution around the F atom outside the van der Waals radii than those of $10a_1$ and $8a_1$ orbitals. As a result, larger attractive interaction was expected for $11a_1$ and $9a_1$ orbitals, since attractive interaction was widely distributed (−60° to +60°) around the F atom as shown in Figure 13b. It has also been found that attractive region was widely distributed (−90° ∼ +90°) with respect to the C−F bond axis) around the direction of the C−F bond axis in the Li−C_2H_5F system.[20] In addition to the above fact, $11a_1$ and $9a_1$ orbitals have smaller electron distribution around the C−H bonds, which shows the repulsive interaction with the metastable atoms, than those of $10a_1$ and $8a_1$ orbitals. As a consequence, absolute values of the slope in CEDPICS for $11a_1$ and $9a_1$ bands become larger than those for $10a_1$ and $8a_1$ bands. Although $7b_2$, $8b_2$, and $9b_2$ orbitals has the same symmetry, electron distribution of the orbital is quite different from each other. The $7b_2$ orbital has larger electron distribution outside the molecular surface around the C−F bond axis with resultant negative slope parameter. $9b_2$ and $8b_2$ bands give positive slope parameters. It is evidenced that the $8b_2$ orbital shows the strongest repulsive interaction with He*. This results from the larger exterior electron distributions having repulsive character around the C−H bonds. This is consistent with the positive ΔE. The observed positive slopes of $9b_2$ and $8b_2$ bands are consistent with the calculated repulsive interaction for the in-plane perpendicular approach with respect to C−F axis (▲) in Figure 13.

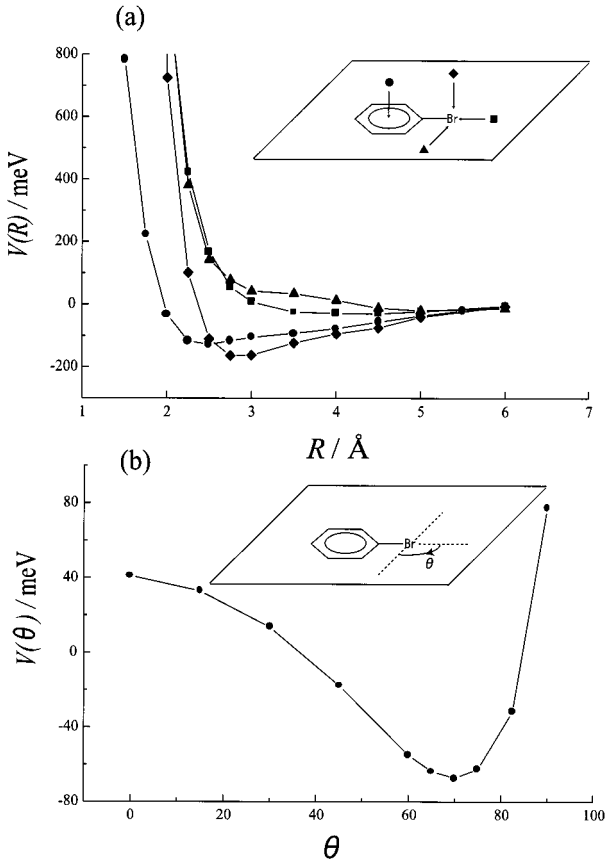

Figure 15. (a) Interaction potential curves $V(R)$ obtained by MP2 calculations for C_6H_5Br and Li as a function of distance R; out-of-plane access to the center of the benzene ring (●); in-plane collinear access to the C−Br bond (■); in-plane perpendicular access to the C−Br axis (▲); out-of-plane perpendicular access to the C−Br axis (◆). Note that R is defined from the center of the benzene ring for (●) direction, while for the others (■), (▲), (◆) R is defined from the Br atom. (b) Interaction potential curve $V(\theta)$ as a function of the in-plane angle θ of ∠Li−Br−C. Distance between Li and Br atoms is fixed at 2.75 Å.

B. Chlorobenzene. Negative m and ΔE, which indicate attractive interaction, were obtained for $2b_1(\pi_1)$ band. Slope parameter of this band is slightly larger compared with that of C_6H_5F. This is due to the fact that the out-of-plane perpendicular approach of He* to C−Cl bond axis (◆) gives the most attractive interaction as shown in Figure 14, while this direction approach for C_6H_5F turns out to be repulsive. In addition to the above fact, the phase of p atomic orbitals for six C atoms and Cl atom is identical with the resultant widely distributed electron distribution. The other π bands such as $\pi_2(1a_2)$ and $\pi_3(4b_1)$ show large slope parameters because of the attractive interaction. Small slope parameters for $8b_2$, $7b_2$, and $12a_1$ bands result from large repulsive interaction around the C−H bonds. The slope parameter of the $14a_1$ band shows a relatively small value (−0.03) despite the larger electron distribution around the collinear direction to the C−Cl axis. This implies that collinear approach of He* to the C−Cl axis is not strongly attractive. Ab initio MO calculation predicted that this direction (■) was repulsive. Bands of $15a_1$ and $13a_1$ orbitals show larger negative slope parameters (−0.17, −0.16), since these orbitals are similar to each other. It may indicate that the origin of these interactions is attractive interaction around the Cl atom centered at ∼65° of ∠Li−X−C angle, while theoretical calculation does not show any attractive interaction because of the neighboring H atoms for this direction as shown in Figure 14b. However, the most attractive interaction has been found around the direction of ±60° with respect to the C−Cl axis in the Li−C_2H_5Cl system.[20] It is also noted that Figure 14b shows the potential well causing the attractive interaction for ∼65° direction. Furthermore, a larger negative slope parameter (−0.21) was obtained for the $9b_2$ band, which has a very large electron distribution around the in-plane sideways direction to the C−Cl axis, as illustrated in Figure 10. Therefore, it is concluded that in-plane sideways approach to C−Cl axis should be governed by the attractive interaction. These findings suggest that further larger basis set will appropriately predict the attractive interaction around this direction. On the other hand, attractive interaction for out-of-plane perpendicular direction (◆) as shown in Figure 14a was obtained from both experiment and theoretical calculation.

C. Bromobenzene. The slope parameters for all bands show negative values. In particular, it is noted that large values of bands 1, 2, 3, 4, and 7 reflect the large and strong attractive force owing to π and/or n orbitals. These values are slightly larger than those of C_6H_5Cl. It is noted that calculated well depth (−165 meV) of the out-of-plane perpendicular approach of He* to the C−Br axis (◆) in Figure 15, which corresponds to band 4 ($n_\perp$), shows good agreement with the observed ΔE (−150 ± 60 meV). Small values of bands 8, 9, and 12 can arise from the larger repulsive orbital contributions around the C−H bonds. Relatively larger slope parameters (−0.18, −0.15, and −0.21) are obtained for bands 5, 10 and 11. These negative values arise from attractive interaction around the in-plane perpendicular direction with respect to the C−Br axis in accord with the observation in the case of C_6H_5Cl. In Figure 15b, theoretical calculation predicted attractive interaction around the in-plane sideways approach ranged from 35 ± 2° to 83 ± 1° with respect to the C−Br bond axis. It is noted that these changes of wideness of attractive region/cone from C_6H_5Cl to C_6H_5Br should be related to the enlargement of the distribution of the halogen orbitals.

D. Iodobenzene. As before, the π and n orbitals show strong attractive interactions. The change in the degrees of the slope parameters on going from C_6H_5F to C_6H_5I are obtained, and they will be discussed in the next section. Since C_6H_5I has an electronic structure similar to that of C_6H_5Cl and C_6H_5Br, similar slope parameters are obtained for the other bands.

CEDPICS and Anisotropic Interaction. As mentioned in the introductory section, CEDPICS of each band reflects the interaction between the reagents in the collision event. The interaction can be divided into an attractive and a repulsive one. If the interaction arises only from either attractive or repulsive effect, ionization cross section decreases or increases with increasing the collision energy, respectively. However, most cases are not so simple, since the electron distribution of a target MO has anisotropic distribution. In other word, a target MO has both an attractive and repulsive part for the approach of the metastable atoms. Then, observed CEDPICS contains the whole interaction around the target MOs. Therefore, if both types of interactions contribute to a large extent, a nonmonotonic feature should be observed in the CEDPICS.

It is easily seen that the $11a_1$ and $8a_1$ band for C_6H_5F consist of two components. Steep slopes of the CEDPICS for lower collision energy arise from attractive interaction around the collinear direction to the C−F bond axis, while the CEDPICS for higher collision energy region can be ascribed to repulsive interaction, which widely expands over the C−H bonds. In the line of the same argument, bands 5 and 8 for C_6H_5Cl and C_6H_5-Br consist of attractive and repulsive interactions. On the other hands, bands 3 for C_6H_5Cl, C_6H_5Br, and C_6H_5I shows the monotonic decrease, which mainly comes from attractive

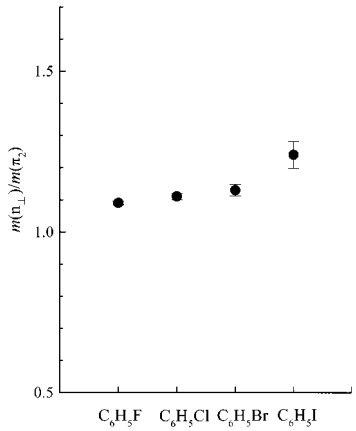

Figure 16. The relative slope parameter of the $n_\perp$ orbitals with respect to the π_2, $m(n_\perp)/m(\pi_2)$ for C_6H_5X (X = F, Cl, Br, I).

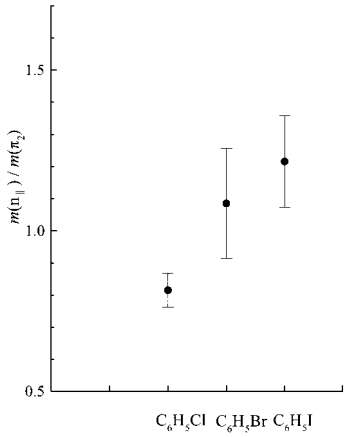

Figure 17. The relative slope parameter of the $n_\parallel$ orbitals with respect to the π_2, $m(n_\parallel)/m(\pi_2)$ for C_6H_5X (X = F, Cl, Br, I).

interaction around the in-plane perpendicular direction with respect to the C−X bond axis. Attractive interaction localized around 65° of the Li−C−X angle as can be seen in Figures 14b and 15b. It is noted that CEDPICS of bands 12 for C_6H_5F and C_6H_5I are similar to each other, which results from both attractive and repulsive interactions. This finding indicates that for C_6H_5I the attractive interaction is localized around the collinear direction to the C−I bond as well as that for C_6H_5F. Contrary, CEDPICS of bands 12 for C_6H_5Cl and C_6H_5Br consist of a single component, which can be ascribed to the repulsive interaction. Then, collinear direction for C_6H_5Cl and C_6H_5Br shows repulsive interaction.

Relative Reactivity of Orbitals with Metastable Atoms. In this section, we will discuss the relative reactivity of the π and n orbitals of monohalogenobenzenes upon electrophilic attack by metastable helium atoms on the basis of the slope parameters of the π and n bands in the CEDPICS. Since C_6H_5-Cl, C_6H_5Br, and C_6H_5I have similar electronic structures, the orbital reactivities are considered mainly among them, although that of C_6H_5F is referred to occasionally. The slope parameters were averaged typically two sets of measurements to eliminate the experimental errors. The relative slope parameters of each compound were obtained with respect to the slope parameter of the π_2 band as a reference in order to minimize systematic errors. Because the π_2 orbital does not mix with the other orbitals owing to difference in symmetry, and also it is not shielded effectively by other orbitals from the attack of the metastable atoms.

(i) Reactivity of n Orbitals. Figure 16 shows the relative slope parameters of the $n_\perp$ band with respect to the π_2 band for C_6H_5X (X = F, Cl, Br, I). As can be seen from Figure 16, attractive interaction around the $n_\perp$ orbitals region is larger than that for the π_2. This is because the $n_\perp$ orbitals, which are mainly generated from the halogen *n*p orbitals (n = 3, 4, 5), extend further outside the molecular surface than the π_2 orbital due to the carbon 2p orbitals except for the F atom. It is noted that these orbitals are well correlated to the out-of-plane perpendicular He* access to the C−X axis (◆) in Figures 13−15. Then the $n_\perp$ orbitals are not effectively shielded by the benzene ring. Slightly larger attractive interaction of the $n_\perp$ orbital for C_6H_5F is a little puzzling here, since ab initio MO calculation predicted repulsive interaction for this direction. However, an electron density map of this orbital indicated in the right side of Figure 9 implies that this orbital has π character localized at the C−F bond, which may be responsible for the attractive interaction of this orbital.

Figure 17 shows the relative slope parameter of the $n_\parallel$ with respect to the π_2 for C_6H_5X (X = Cl, Br, I). As was mentioned before, the $n_\parallel$ orbitals are shielded by the benzene ring from the attack of the metastables. This shielding effect is strong for C_6H_5Cl and becomes much weaker for larger *n* orbitals.

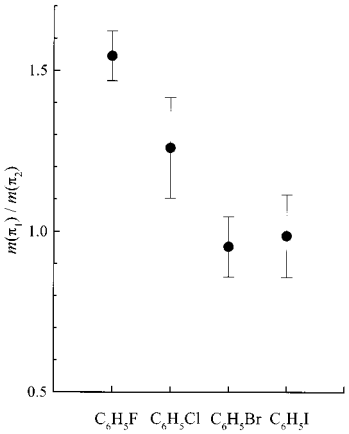

Figure 18. The relative slope parameter of the π_1 orbitals with respect to the π_2, $m(\pi_1)/m(\pi_2)$ for C_6H_5X (X = F, Cl, Br, I).

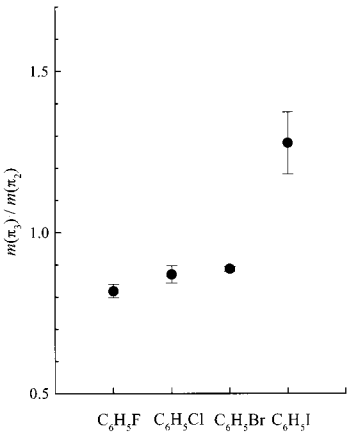

Figure 19. The relative slope parameter of the π_3 orbitals with respect to the π_2, $m(\pi_3)/m(\pi_2)$ for C_6H_5X (X = F, Cl, Br, I).

(ii) Reactivity of π Orbitals. Figures 18 and 19 show the relative slope parameters of the π_1 and π_3 bands with respect to the π_2 band for C_6H_5X (X = Cl, Br, I). It is found from the figures that the attractive interaction for the π_1 bands decreases and those for the π_3 increases on going from C_6H_5Cl to C_6H_5I. These changes can be interpreted in terms of the changes of halogen *n*p orbital contribution to the orbitals π_1 and π_3. The π_1 and π_3 orbitals of the benzene interact with the out-of-plane halogen *n*p orbitals. As can be seen in Figure 20, the halogen

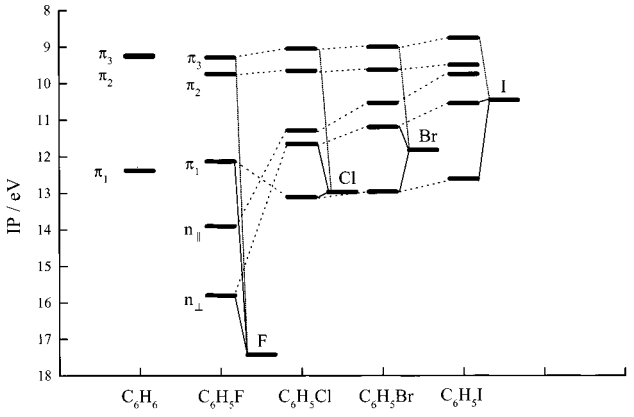

Figure 20. Correlation energy diagram for the π and n orbitals of C_6H_5X (X = F, Cl, Br, I).

*n*p orbital character in the π_1 orbitals decreases with increasing *n*, namely from Cl to I. The fact that the relative slope parameter of the π_1 orbitals in Figure 18 decreases from C_6H_5Cl to C_6H_5I despite the increase in the size of the perpendicular component of halogen p orbital shows that the effect of the p orbital mixing is larger than that of the p orbital size effect on the anisotropic interaction of the π_1 orbital. On the other hand, the halogen *n*p orbital character in the π_3 orbitals increases from Cl to I, since the ionization potential of the halogen atom is getting closer to the π_3 in benzene on going from Cl to I. This p orbital size effect explains the increment of the reactivity and the attractive interaction of the π_3 orbitals. It is also noted that as the energy level of the HOMO becomes higher, its interaction with the He* becomes more effective to give attractive interactions as in accordance with the case of substituted ethylenes.[15]

VI. Conclusion

In this study, the results of PIES of C_6H_5X (X = F, Cl, Br, I) with metastable He*(2^3S) atom were presented. Highly anisotropic interactions around halogen atoms are obtained. Attractive interaction was dominated around the collinear access of He*(2^3S) to C−F axis in C_6H_5F. On the other hand, attractive interaction was localized around the out-of-plane perpendicular approach of He* atom to C−X (X = Cl, Br, I). It is also found that the π orbitals show attractive interactions for these compounds. The most attractive interaction for these compounds increases on going from C_6H_5Cl to C_6H_5I. Furthermore, we discussed the magnitude of the attractive interaction of the π and n orbitals of monohalogenobenzenes upon electrophilic attack by the He* atoms on the basis of the peak energy shifts and the relative slope parameters of CEDPICS for the π and n orbitals in the 2D-PIES. It is found that the anisotropic interaction depends on the electronic factor due to the size of the halogen p orbitals and the conjugation between the benzene ring and the halogen atoms, and also on the steric factor due to the benzene ring shielding some orbitals from the impact of metastable atoms.

Acknowledgment. This work has been partially supported by a Grant in Aid for Scientific Research from the Japanese Ministry of Education, Science, and Culture. One of the authors (K.I.) thanks the Japan Society for the Promotion of Science (JSPS) for a JSPS Research Fellowship.

References and Notes

(1) Penning, F. M. *Naturwissenschaften* **1927**, *15*, 818.
(2) Hotop, H.; Niehaus, A. *Z. Phys*. **1969**, *228*, 68.
(3) Ohno, K.; Mutoh, H.; Harada, Y. *J. Am. Chem. Soc*. **1983**, *105*, 4555.
(4) Ohno, K.; Matsumoto, S.; Harada, Y. *J. Chem. Phys*. **1984**, *81*, 4447.
(5) Siska, P. E. *Rev. Mod. Phys*. **1993**, *65*, 337, and references therein.
(6) Yamakado, H.; Yamaguchi, M.; Hoshino, S.; Ohno, K. *J. Phys. Chem*. **1995**, *99*, 55.
(7) Ohno, K.; Yamakado, H.; Ogawa, T.; Yamata, T. *J. Chem. Phys*. **1996**, *105*, 7536.
(8) Takami, T.; Ohno, K. *J. Chem. Phys*. **1992**, *96*, 6523.
(9) Yamauchi, M.; Yamakita, Y.; Yamakado, H.; Ohno, K. *J. Electron Spectrosc. Relat. Phenom*. **1998**, *88*−*91*, 155.
(10) Kishimoto, N.; Yamakado, H.; Ohno, K. *J. Phys. Chem. A* **1996**, *100*, 8204.
(11) Yamakita, Y.; Yamauchi, M.; Ohno, K. *Chem. Phys. Lett*. **2000**, *322*, 189.
(12) Kishimoto, N.; Ohno, K. *J. Phys. Chem. A* **2000**, *104*, 6940.
(13) Kishimoto, N.; Furuhashi, M.; Ohno, K. *J. Electron Spectrosc. Relat. Phenom*. **2000**, *113*, 35.
(14) Ohno, K.; Kishimoto, N.; Yamakado, H. *J. Phys. Chem*. **1995**, *99*, 9687.
(15) Yamakado, H.; Okamura, K.; Ohshimo, K.; Kishimoto, N.; Ohno, K. *Chem. Lett*. **1997**, 269.
(16) Kishimoto, N.; Ohshimo, K.; Ohno, K. *J. Electron Spectrosc. Relat. Phenom*. **1999**, *104*, 145.
(17) Takami, T.; Mitsuke, K.; Ohno, K. *J. Chem. Phys*. **1991**, *95*, 918.
(18) Tokue, I.; Sakai, Y.; Yamasaki, K. *J. Chem. Phys*. **1997**, *106*, 4491.
(19) Alberti, M.; Lucas, J. M.; Brunetti, B.; Pirani, F.; Stramaccia, M.; Rosi, M.; Vecchiocattivi, F. *J. Phys. Chem. A* **2000**, *104*, 1405.
(20) Imura, K.; Kishimoto, N.; Ohno, K. *J. Phys. Chem. A*, submitted for publication.
(21) Mitsuke, K.; Takami, T.; Ohno, K. *J. Chem. Phys*. **1989**, *91*, 1618.
(22) Ohno, K.; Takami, T.; Mitsuke, K.; Ishida, T. *J. Chem. Phys*. **1991**, *94*, 2675.
(23) Gardner, J. L.; Samson, J. A. R. *J. Electron Spectrosc. Relat. Phenom*. **1976**, *8*, 469.
(24) Kimura, K.; Katsumata, S.; Achiba, Y.; Yamazaki, T.; Iwata, S. *Handbook of He I Photoelectron Spectra of Fundamental Organic Molecules*; Japan Scientific: Tokyo, 1981.
(25) Turner, D. W.; Baker, C.; Baker, A. D.; Brundle, C. R. *Molecular Photoelectron Spectroscopy*; Wiley: London, 1970.
(26) Yee, D. S. C.; Stewart, W. B.; Mcdowell, C. A.; Brion, C. E. *J. Electron Spectrosc. Relat. Phenom*. **1975**, *7*, 93.
(27) Hotop, H.; Hubler, G. *J. Electron Spectrosc. Relat. Phenom*. **1977**, *11*, 101.
(28) (a) Auerbach, D. J. *Atomic and Molecular Beam Methods*; Scoles, G., Ed.; Oxford University: New York, 1988; p 369. (b) Kishimoto, N.; Aizawa, J.; Yamakado, H.; Ohno, K. *J. Phys. Chem. A* **1997**, *101*, 5038.
(29) Doraiswamy, S.; Sharma, S. *J. Mol. Struct*. **1983**, *102*, 1594.
(30) Rosental, E.; Dailey, B. P. *J. Chem. Phys*. **1965**, *43*, 2093.
(31) Michel, F.; Nery, H. Roussy, G. *Compt. Rend*. **1974**, *278B*, 203.
(32) Brunvoll, J.; Samdal, S.; Thomassen, H.; Vilkov, L. V.; Volden, H. V. *Acta Chem. Scand*. **1990**, *44*, 23.
(33) Pauling, L. *The Nature of the Chemical Bond*; Cornell University: Ithaca, New York, 1960.
(34) Rothe, E. W.; Neynaber, R. H.; Trujillo, S. M. *J. Chem. Phys*. **1965**, *42*, 3310.
(35) Illenberger, E.; Niehaus, A. *Z. Phys. B* **1975**, *20*, 33.
(36) Parr, T.; Parr, D. M.; Martin, R. M. *J. Chem. Phys*. **1982**, *76*, 316.
(37) Hotop, H. *Radiat. Res*. **1974**, *59*, 379.
(38) Haberland, H.; Lee, Y. T.; Siska, P. E. *Adv. Chem. Phys*. **1981**, *45*, 487.
(39) Frisch, M. J.; Trucks, G. W.; Schlegel, H. B.; Scuseria, G. E.; Robb, M. A.; Cheeseman, J. R.; Zakrzewski, V. G.; Montgomery, J. A., Jr.; Stratmann, R. E.; Burant, J. C.; Dapprich, S.; Millam, J. M; Daniels, A. D.; Kudin, K. N.; Strain, M. C.; Farkas, O.; Tomasi, J.; Barone, V.; Cossi, M.; Cammi, R.; Mennucci, B.; Pomelli, C.; Adamo, C.; Clifford, S.; Ochterski, J.; Petersson, G. A.; Ayala, P. Y.; Cui, Q.; Morokuma, K.; Malick, D. K.; Rabuck, A. D.; Raghavachari, K.; Foresman, J. B.; Cioslowski, J.; Ortiz, J. V.; Baboul, A. G.; Stefanov, B. B.; Liu, G.; Liashenko, A.; Piskorz, P.; Komaromi, I.; Gomperts, R.; Martin, R. L.; Fox, D. J.; Keith, T.; Al-Laham, M. A.; Peng, C. Y.; Nanayakkara, A.; Challacombe, M.; Gill, P. M. W.; Johnson, B.; Chen, W.; Wong, M. W.; Andres, J. L.; Gonzalez, C.; Head-Gordon, M.; Replogle, E. S.; Pople, J. A. *GAUSSIAN 98*; Gaussian, Inc.: Pittsburgh, PA, 1998.
(40) von Niessen, W.; Schirmer, J.; Cederbaum, L. S. *Comput. Phys. Rep*. **1984**, *1*, 57.
(41) (a) Zakrewski, V. G.; Ortiz, J. V. *Int. J. Quantum Chem. Symp*. **1994**, *28*, 23. (b) Zakrewski, V. G.; Ortiz, J. V. *Int. J. Quantum Chem. Symp*. **1995**, *53*, 583.
(42) Potts, A. W.; Lyus, M. L.; Lee, E. P. F.; Fattahallah, G. H. *J. Chem. Soc., Faraday Trans. 2* **1980**, *76*, 556.

(43) Ruščic, B.; Klasnic, L.; Wolf, A.; Knop, J. V. *J. Phys. Chem*. **1981**, *85*, 1486.
(44) von Niessen, W.; Åsbrink, L.; Bieri, G. *J. Electron Spectrosc. Relat. Phenom*. **1982**, *26*, 173, and references therein.
(45) Fujisawa, S.; Ohno, K.; Masuda, S.; Harada, Y. *J. Am. Chem. Soc*. **1986**, *108*, 6505.
(46) Munakata, T.; Harada, Y.; Ohno, K.; Kuchitsu, K. *Chem. Phys. Lett*. **1981**, *84*, 6.
(47) Ohno, K.; Fujisawa, S.; Mutoh, H.; Harada, Y. *J. Phys. Chem*. **1982**, *86*, 440.
(48) Harada, Y.; Ohno, K.; Mutoh, H. *J. Chem. Phys*. **1983**, *79*, 3251.